Interpolation over Light Fields with Applications in Computer Graphics*

F. Betul Atalay† David M. Mount‡

Abstract

We present a data structure, called a *ray interpolant tree*, or *RI-tree*, which stores a discrete set of directed lines in 3-space, each represented as a point in 4-space. Each directed line is associated with some small number of continuous geometric attributes. We show how this data structure can be used for answering *interpolation queries*, in which we are given an arbitrary ray in 3-space and wish to interpolate the attributes of neighboring rays in the data structure. We illustrate the practical value of the RI-tree in two applications from computer graphics: ray tracing and volume visualization. In particular, given objects defined by smooth curved surfaces, the RI-tree can produce high-quality renderings significantly faster than standard methods. We also investigate a number of tradeoffs between the space and time used by the data structure and the accuracy of the interpolation results.

1 Introduction

There is a growing interest in algorithms and data structures that combine elements of discrete algorithm design with continuous mathematics. This is particularly true in computer graphics. Consider for example the process of generating a photo-realistic image. The most popular method for doing this is *ray-tracing* [12]. Ray-tracing models the light emitted from light sources as traveling along rays in 3-space. The color of a pixel in the image is a reconstruction of the intensity of light traveling along various rays that are emitted from a light source, transmitted and reflected among the objects in the scene, and eventually entering the viewer's eye.

There are many different methods for mapping this approach into an algorithm. At an abstract level, all ray-tracers involve forming an image by combining various continuous quantities, or *attributes*, that have been generated from a discrete set of sampled rays. These continuous attributes include color, radiance, surface normals, and reflection and refraction vectors. These attributes vary continuously either as a function of the location on the surface of an object or as a function of the location of the viewer and the locations of the various light sources in 3-space. The reconstruction process involves combining various discretely sampled attributes in the context of some illumination model.

Producing images by ray-tracing is a computationally intensive process. The degree of realism in the final image depends on a number of factors, including the density and number of samples that are used to compute a pixel's intensity and the fidelity of the illumination model to the physics of illumination. Scenes can involve hundreds of light sources and from thousands to millions of objects, often represented as smooth surfaces, including implicit surfaces [6], subdivision surfaces [22], and Bezier surfaces and NURBS [9]. Reflective and transparent objects cause rays to be reflected and refracted, further increasing the numbers of rays that need to be traced. In traditional ray-tracing solutions, each ray is traced through the scene as needed to compute the intensity of a pixel in the image [12]. Much of the work involves determining the first object that is intersected by each ray and the location that the ray hits.

In this paper, we propose one approach to help to accelerate this process by reducing the number of intersection calculations. Our algorithm facilitates fast, approximate rendering of a scene from any viewpoint, and is most useful when the scene is rendered from multiple viewpoints, as arises in computing animations. Rather than tracing each input ray to compute the required attributes, we collect and store a relatively sparse set of *sampled rays* based on demand and associate some continuous geometric attributes with each sample in a fast data structure. We can then use inexpensive *interpolation* methods to approximate the value of these sampled quantities for other input rays. Using an adaptive strategy, it is possible to avoid oversampling in smooth areas while providing sufficiently dense sampling in regions of high variation. We dynamically maintain a *cache* of the most recently generated samples, in order to reduce the space requirements of the data structure.

The information associated with a given ray is indexed according to the directed line that supports the ray, which in turn is modeled as a point in a 4-dimensional *line space*. Given a ray to be traced, we access the data structure to locate a number of neighboring sampled rays in line space. We then interpolate the continuous information from the

*This material is based upon work supported by the National Science Foundation under Grant No. 0098151.

†Department of Computer Science, University of Maryland, College Park, Maryland. Email: betul@cs.umd.edu.

‡Department of Computer Science and Institute for Advanced Computer Studies, University of Maryland, College Park, Maryland. Email: mount@cs.umd.edu.

neighboring rays. The resulting data structure is called an *RI-tree* or *ray interpolant tree*.

1.1 Related Work The idea of associating radiance information with points in line space has a considerable history, dating back to work in the 1930's by Gershun on vector irradiance fields [10] and Moon and Spencer's concept of photic fields [17], and more recent papers by Levoy and Hanrahan [16] and Gortler, Grzeszczuk, Szeliski, and Cohen [13]. The term "light field" in our title was coined by Levoy and Hanrahan, but our notion is more general than theirs because we consider interpolation of any continuous information, not just radiance. Most methods for storing light field information in computer graphics are based on discretizing the space into uniform grids. In contrast, we sample rays adaptively, concentrating more samples where they are greatest value. The most closely related work to ours is the Interpolant Ray-tracer system introduced by Bala, Dorsey, and Teller [4], which combines adaptive sampling of radiance information, caching, and interpolation for rendering convex objects. Our method generalizes theirs by storing ad interpolating not only radiance information but other sorts of continuous information, which may be relevant to the rendering process. We also allow nonconvex objects. Unlike their method, however, we do not provide guarantees on the worst-case approximation error.

In addition, there has been earlier research on accelerating ray tracing by reducing the cost of intersection computations using bounding volume hierarchies [19], space partitioning structures [11, 15], and methods exploiting ray coherence [2, 14, 1, 18]. Some of these methods can be applied in combination with ours.

A simpler variant of this data structure was introduced by the authors in [3]. The current data structure has two main improvements over the previous one. Firstly, the previous data structure was not *dynamic*: as a pre-processing phase, the entire data structure was built sampling millions of rays originating from the entire space of viewpoints in various directions. This resulted in high pre-processing times, and high space requirements. The current data structure, on the other hand, is dynamically built generating samples on demand—only when they are actually needed, and maintained by a caching mechanism. Secondly, the current system generalizes the framework and can handle general scenes containing multiple objects with different surface reflectance properties, whereas the previous system focused on single reflective or transparent objects. In addition, a systematic analysis of the performance of the data structure is presented in this paper.

1.2 Design Issues The approach of computing a sparse set of sample rays and interpolating the results of ray shooting is most useful for rendering smooth objects that are reflective or transparent, for rendering animations when the viewpoint varies smoothly, and for generating high-resolution images and/or antialiased images generated by supersampling [12] in which multiple rays are shot for each pixel of the image.

Although we have motivated the RI-tree data structure from the perspective of ray-tracing, there are a number of applications having to do with lines in 3-space that can benefit from this general approach. To illustrate this, we have studied two different applications, one involving image generation through ray-tracing and the other involving volume visualization with applications in medical imaging for radiation therapy.

There are a number of issues that arise in engineering a practical data structure for interpolation in line space. These include the following.

How and where to sample rays? Regions of space where continuous information varies more rapidly need to be sampled with greater density than regions that vary smoothly.

Whether to interpolate? In the neighborhood of a discontinuity, the number of rays that may need to be sampled to produce reasonable results may be unacceptably high. Because the human eye is very sensitive to discontinuities near edges and silhouettes, it is often wise to avoid interpolating across discontinuities. This raises the question of how to detect discontinuities. When they are detected, is it still possible to interpolate or should we avoid interpolation and use standard ray-tracing instead?

How many samples to maintain? Even for reasonably smooth scenes, the number of sampled rays that would need to be stored for an accurate reconstruction runs well into millions. For this reason, we *cache* the results of only the most relevant rays. What are the space-time tradeoffs involved with this approach?

We investigate these and other questions in the context of a number of experiments based on the applications mentioned above. The paper is organized as follows. In the rest of this section, we give a brief overview of our algorithm in the context of ray-tracing. In Section 2, we explain the construction of our data structure, and its use for answering *interpolation queries*. In Section 3, we report experimental results.

1.3 Algorithm Overview In order to make things concrete, we will describe our data structure in terms of a ray-tracing application. As mentioned in the introduction, ray-tracing works by simulating the light propagation in a scene. A traditional ray-tracer shoots one or more rays from the viewpoint through each pixel of the image plane. The ray is traced through the scene and the intensity gathered constitutes the color of that pixel. To reduce problems of aliasing,

multiple rays may also be traced for each pixel and these results are interpolated.

We can distinguish two major tasks in a ray-tracer. The *geometric component* is responsible for calculating the closest visible object point along a specific ray, as the *shading component* computes the color of that point. If the object is reflective or transparent, the reflection and transmission rays are traced recursively to gather their contribution to the intensity. The primary expense in ray-tracing lies in the geometric component, especially for scenes that contain complex objects such as Bezier or NURBS surfaces, and/or reflective and refractive objects.

Each object can be modeled abstractly as a function f mapping input rays to a set of geometric attributes that are used in color computation. The attributes depend on the object's surface reflectance properties. For objects whose surfaces are neither reflective nor transparent, denoted *simple surfaces*, the function returns the point of intersection and the surface normal at this point. For objects whose surfaces are either reflective or transparent the function additionally returns the *exit ray*, that is, the reflected or refracted ray, respectively, that leaves the object's surface. The exit ray is represented by its origin, the *exit point*, and directional *exit vector*. In general, objects that are both reflective and refractive could be handled by associating multiple exit rays with an input ray, but our implementation currently does not support this. These quantities are depicted in Fig. 1 and the function is described schematically below. We will refer to the combination of the underlined attributes below as the *output ray*.

For simple surfaces:
f : Ray $\rightarrow$ {Normal,IntersectionPoint}

Otherwise:
f : Ray $\rightarrow$ {Normal,IntersectionPoint,ExitPoint,ExitVector}

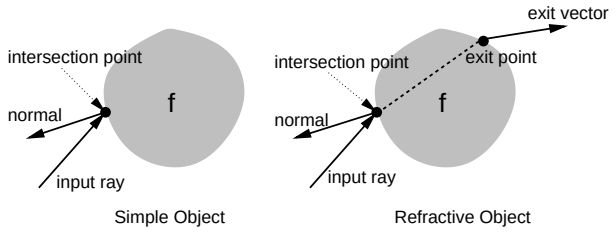

Figure 1: Geometric attributes.

For many real world objects, which have large smooth surfaces, f is expected to vary smoothly. In the context of ray-tracing, this is referred to as *ray coherence*. Nearby rays follow similar paths, hit nearby points having similar normal vectors and hence are subject to similar reflections and/or refractions. In the neighborhood of discontinuities, however, nearby input rays may follow quite different paths. In cases where we cannot find sufficient evidence to interpolate, we perform ray-tracing instead.

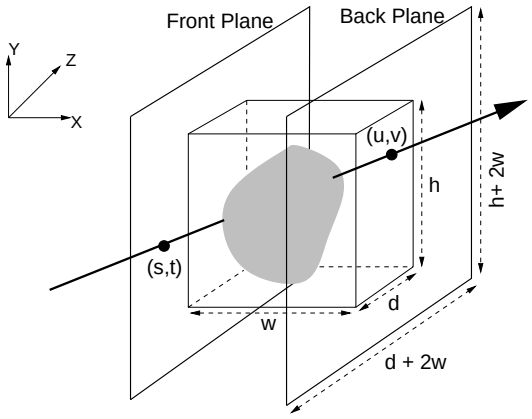

Figure 2: The two-plane parameterization of directed lines and rays. The +X plane pair is shown.

In a traditional ray-tracer, each object is associated with a procedure that computes intersections between rays and this object. For objects whose boundaries are sufficiently smooth, we replace this intersection procedure with a data structure, which will be introduced in the next section. This data structure approximates the function f through interpolation.

2 The Ray Interpolant Tree

In this section we introduce the main data structure used in our algorithm, the *RI-tree* or *ray interpolant tree*. Each RI-tree is associated with a single *object* of the scene, which is loosely defined to be a collection of logically related surfaces. The object is enclosed by an axis-aligned bounding box. The data structure stores the geometric attributes associated with some set of sampled rays, which may originate from any point in space and intersect the object's bounding box.

2.1 Parameterizing Rays as Points We will model each ray by the directed line that contains the ray. Directed lines can be represented as a point lying on a 4-dimensional manifold in 5-dimensional projective space using Plücker coordinates [21], but we will adopt a simpler popular representation, called the *two-plane parameterization* [13, 16, 4]. A directed line is first classified into one of 6 different classes (corresponding to 6 *plane pairs*) according to the line's *dominant direction*, defined to be the axis corresponding to the largest coordinate of the line's directional vector and its sign. These classes are denoted $+X, -X, +Y, -Y, +Z, -Z$. The directed line is then represented by its two intercepts (s, t)

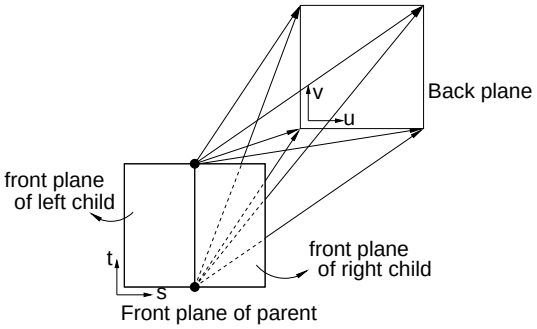

Figure 3: Subdivision along s-axis.

and (u, v) with *front plane* and *back plane*, respectively, that are orthogonal to the dominant direction and coinciding with the object's bounding box. For example, as shown in Fig. 2, ray R with dominant direction $+X$ first intersects the front plane of the $+X$ plane pair at (s, t), and then the back plane at (u, v), and hence is parameterized as (s, t, u, v). Note that, the $+X$ and $-X$ involve the same plane pair but differ in the distinction between front and back plane.

2.2 The RI-tree The RI-tree is a binary tree based on a recursive subdivision of the 4-dimensional space of directed lines. It consists of six separate 4-dimensional kd-trees [5, 20] one for each of the six dominant directions. The root of each kd-tree is a 4-dimensional hypercube in line space containing all rays that are associated with the corresponding plane pair. The 16 corner points of the hypercube represent the 16 rays from each of the four corners of the front plane to the each of the four corners of the back plane. Each node in this data structure is associated with a 4-dimensional hyperrectangle, called a *cell*. The 16 corner points of a leaf cell constitute the ray samples, which form the basis of our interpolation. When the leaf cell is constructed, these 16 rays are traced and the associated geometric attributes are stored in the leaf.

2.3 Adaptive Subdivision and Cache Structure The RI-tree grows and shrinks dynamically based on demand. Initially only the root cell is built by sampling its 16 corner rays. A leaf cell is is subdivided by placing a cut-plane at the midpoint orthogonal to the coordinate axis with the longest length. In terms of the plane pair, this corresponds to dividing the corresponding front or back plane through the midpoint of the longer side. We partition the existing 16 corner samples between the two children, and sample eight new corner rays that are shared between the two child cells. (These new rays are illustrated in Fig. 3 in the case that the s-axis is split.)

Rays need to be sampled more densely in some regions than others, for example, in regions where geometric attributes have greater variation. For this reason, the subdivision is carried out adaptively based on the distance between output attributes. The distance between two sets of output attributes are defined as the distance between their associated output rays. We define the *distance* between two rays to be the L_2 distance between their 4-dimensional representations. To determine whether a cell should be subdivided, we first compute the correct output ray associated with the midpoint of the cell, and then we compute an approximate output ray by interpolation of the 16 corner rays for the same point. If the distance between these two output rays exceeds a given user-defined *distance threshold* and the depth of the cell in the tree is less than a user-defined *depth constraint*, the cell is subdivided. Otherwise the leaf is said to be *final*.

If we were to expand all nodes in the tree until they are final, the resulting data structure could be very large, depending on the distance threshold and the depth constraint. For this reason we only expand a node to a final leaf if this leaf node is needed for some interpolation. Once a final leaf node is used, it is marked with a time stamp. If the size of the data structure exceeds a user-defined *cache size*, then the the tree is pruned to a constant fraction of this size by removing all but the most recently used nodes. In this way, the RI-tree behaves much like an LRU-cache.

2.4 Rendering and Interpolation Queries Recall that our goal is to use interpolation between sampled output rays whenever things are sufficiently smooth. RI-tree can be used to perform a number of functions in rendering, including determining the first object that a ray hits, computing the reflection or refraction (exit) ray for nonsimple objects, and answering various visibility queries, which are used for example to determine whether a point is visible to a light source or in a shadow.

Let us consider the interpolation of a given input ray R. We first map R to the associated point in the 4-dimensional directed line space and, depending on the dominant direction of this line, we find the leaf cell of the appropriate kd-tree through a standard descent. Since the nodes of the tree are constructed only as needed, it is possible that R will reside in a leaf that is not marked as *final*. This means that this particular leaf has not completed its recursive subdivision. In this case, the leaf is subdivided recursively, along the path R would follow, until the termination condition is satisfied, and the final leaf containing R is now marked as *final*. (Other leaves generated by this process are not so marked.)

Given the final leaf cell containing R, the output attributes for R can now be interpolated. Interpolation proceeds in two steps. First we group the rays in groups of four, which we call the *directional groups*. Rays in the same group originate from the same corner point on the front plane, and pass through each of the four corners of the back plane (For example, Fig. 4 shows the rays that originate from the north-

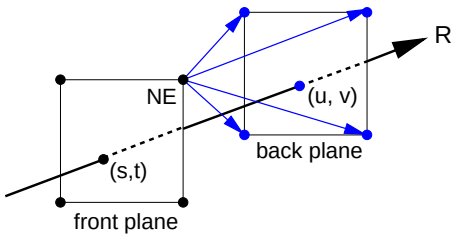

Figure 4: Sampled rays within a directional group.

east corner of the front plane). Within each directional group bilinear interpolation with respect to (u, v) coordinates is performed to compute intermediate output attributes. The outputs of these interpolations are then bilinearly interpolated with respect to (s, t) coordinates to get the approximate output attributes for R. Thus, this is essentially a quadrilinear interpolation.

2.5 Handling Discontinuities and Regions of High Curvature Through the use of interpolation, we can greatly reduce the number of ray samples that would otherwise be needed to render a smooth surface. However, if the ray-output function f contains discontinuities, as may occur at the edges and the outer silhouettes of the object, then we will observe bleeding of colors across these edges. This could be remedied by building a deeper tree, which might involve sampling of rays up to pixel resolution in the discontinuity regions. This would result in unacceptably high memory requirements. Instead our approach will be to detect and classify discontinuity regions. In some cases we apply a more sophisticated interpolation. Otherwise we do not interpolate and instead simply revert to ray-tracing. We will present a brief overview of how discontinuities are handled here. Further details are presented in [3].

Our objects are specified as a collection of smooth surfaces, referred to as *patches*. Each patch is assigned a *patch-identifier*. Associated with each sample ray, we store the patch-identifier of the first patch it hits. Since each ray sample knows which surface element it hits, it would be possible to disallow any interpolation between different surfaces. It is often the case, however, that large smooth surfaces are composed of many smaller patches, which are joined together along edges so that first and second partial derivatives vary continuously across the edge. In such cases interpolation is allowed. We assume that the surfaces of the scene have been provided with this information, by partitioning patches into surface equivalence classes. If the patch-identifiers associated with the 16 corner ray samples of a final leaf are in the same equivalence class, we conclude that there is no discontinuities crossing the region surrounded by the 16 ray hits, and we apply the interpolation process described above.

Requiring that all 16 patches arise from the same equivalence class can significantly limit the number of instances in which interpolation can be applied. After all, linear interpolation in 4-space can be performed with as few as 5 sample points. If the patch-identifiers for the 16 corner samples of the leaf arise from more than two equivalence classes, then we revert to ray tracing. On the other hand, if exactly two equivalence classes are present, implying that there is a single discontinuity boundary, then we perform an intersection test to determine which patch the query ray hits. Let p_r denote this patch. This intersection test is not as expensive as a general tracing of the ray, since typically only a few patches are involved, and only the first level intersections of a ray-tracing procedure is computed. Among the 16 corner ray samples, only the ones that hit a patch in the same equivalence class as p_r are *usable* as interpolants. These are the ray samples hitting the same side of a discontinuity boundary as the query ray. If we determine that there is a sufficient number of *usable* ray samples, we then interpolate the ray. Otherwise, we use ray-tracing. See [3] for further details.

Even if interpolation is allowed by the above criterion, it is still possible that interpolation may be inadvised because the surface has high curvature, resulting in very different output rays for nearby input rays. High variations in the output ray (i.e. normal or the exit ray), signal a discontinuous region. As a measure to determine the distance between two output rays, we use the angular distance between their directional vectors. If any pairwise distance between the output rays corresponding to the usable interpolants is greater than a given *angular threshold*, then interpolation is not performed.

3 Experimental Results

The data structure described in the previous section is based on a number of parameters, which directly influence the algorithm's accuracy and the size and depth of the tree, and indirectly influences the running time. We have implemented the data structure and have run a number of experiments to test its performance as a function of a number of these parameters. We have performed our comparisons in the context of two applications.

Ray-tracing: This has been described in the previous section. We are given a scene consisting of objects that are either simple, reflective or transparent and a number of light sources. The output is a rendering of the scene from one or more viewpoints.

Volume Visualization: This application is motivated from the medical application of modeling the amount of radiation absorbed in human tissue [7]. We wish to visualize the absorption of radiation through a set of nonintersecting objects in 3-space. In the medical application these objects may be models of human organs, bones, and tumors. For visualization purposes,

we treat these shapes as though they are transparent (but do not refract light rays). If we imagine illuminating such a scene by x-rays, then the intensity of a pixel in the image is inversely proportional to the length of its intersection with the various objects of the scene. For each object stored as an RI-tree, the geometric attribute associated with each ray is this intersection length.

We know of no comparable algorithms or data structures with which to compare our data structure. Existing image-based data structures [13, 16] assume a dense sampling of the light field, which would easily exceed our memory resources at the resolutions we would like to consider. The Interpolant Ray-tracer system by Bala, et al. [4] only deals with convex objects, and only interpolates radiance information. Our data structure can handle nonconvex objects and may interpolate any type of continuous attributes.

3.1 Test Inputs We have generated a number of input scenes including different types of objects. As mentioned earlier, for each object in a scene we may choose to represent it in the traditional method or to use our data structure. Our choice of input sets has been influenced by the fact that the RI-tree is most beneficial for high-resolution renderings of smooth objects, especially those that are reflective or transparent. We know of no appropriate benchmark data sets satisfying these requirements, and so we have generated our own data sets.

Bezier Surface: This is a surface is used to demonstrate the results of interpolation algorithm for smooth reflective objects. It consists of a reflective surface consisting of 100 Bezier patches, joined with C^2 continuity at the edges. The surface is placed within a large sphere, which has been given a pseudo-random procedural texture [8]. Experiments run with the Bezier surface have been averaged over renderings of the surface from 3 different viewpoints. Fig. 10(a) shows the Bezier surface from one viewpoint. We rendered images of size 600×600 without anitaliasing (that is, only one ray per pixel is shot.)

Random volumes: We ran another set of experiments on randomly generated refractive, nonintersecting, convex Bezier objects. In order to generate nonintersecting objects, a given region is recursively subdivided into a given number of non-intersecting cells by randomly generated axis-aligned hyperplanes, and a convex object is generated within each such cell. Each object is generated by first generating a random convex planar polyline that defines the silhouette of right half of the object. The vertices of the polyline constitute the control points for a random number (n) of Bezier curves, ranging from 5 to 16. Then a surface of revolution is generated, giving rise to $4n$ Bezier surface patches. The volumes are used both for the ray-tracing and the volume visualization experiments. For ray-tracing we rendered anti-aliased images of size 300×300 (with 9 rays shot per pixel). For volume visualization we rendered 600×600 images without antialiasing. Results are averaged over three different random scenes containing 8, 6, and 5 volumes respectively. Fig. 11 shows a scene of refractive volumes.

Tomatoes: This is a realistic scene used to demonstrate the performance and quality of our algorithm for real scenes. The scene consists of a number of tomatoes, modeled as spheres, placed within a reflective bowl, modeled using Bezier surfaces. This is covered by a reflective and transparent but non-refractive plastic wrap (the same Bezier surface described above). There is a Bezier surface tomato next to the bowl, and they are both placed on a reflective table within a large sphere. The wrap reflects the procedurally textured sphere. The scene is shown in Fig. 9.

3.2 Metrics We investigated the *speedup* and *actual error* committed as a function of four different parameters. Speedup is defined both in terms of number of floating point operations, or *FLOPs*, and CPU-time. FLOP speedup is the ratio of the number of FLOPs performed by traditional ray-tracing to the number of FLOPs used by our algorithm to render the same scene. Similarly, CPU speedup is the ratio of CPU-times. Note that FLOPs and CPU-times for our algorithm include both the sampling and interpolation time.

The actual error committed in a ray-tracing application is measured as the average L_2 distance between the RGB values of corresponding pixels in a ray-traced image and the interpolated image. RGB value is a 3-dimensional vector with values normalized to the range $[0, 1]$. Thus the maximum possible error is $\sqrt{3}$. The error in a volume visualization application is measured as the average distance between the actual length attribute and the corresponding interpolated length attribute.

3.3 Varying the Distance Threshold Recall that the distance threshold, described in Section 2.3, is used to determine whether an approximate output ray and the corresponding actual output ray are close enough (in terms of L_2 distance) to terminate a subdivision process. We varied the distance threshold from 0.01 to 0.25 while the other parameters are fixed. The results for the Bezier surface scenes are shown in Fig. 5.

As expected, the actual error decreases as the threshold is lowered, due to denser sampling. But, the overhead of more sample computations reduces the speedup. However, even for low thresholds where the image quality is high, the CPU-speedup is greater than 2 and the FLOP-speedup

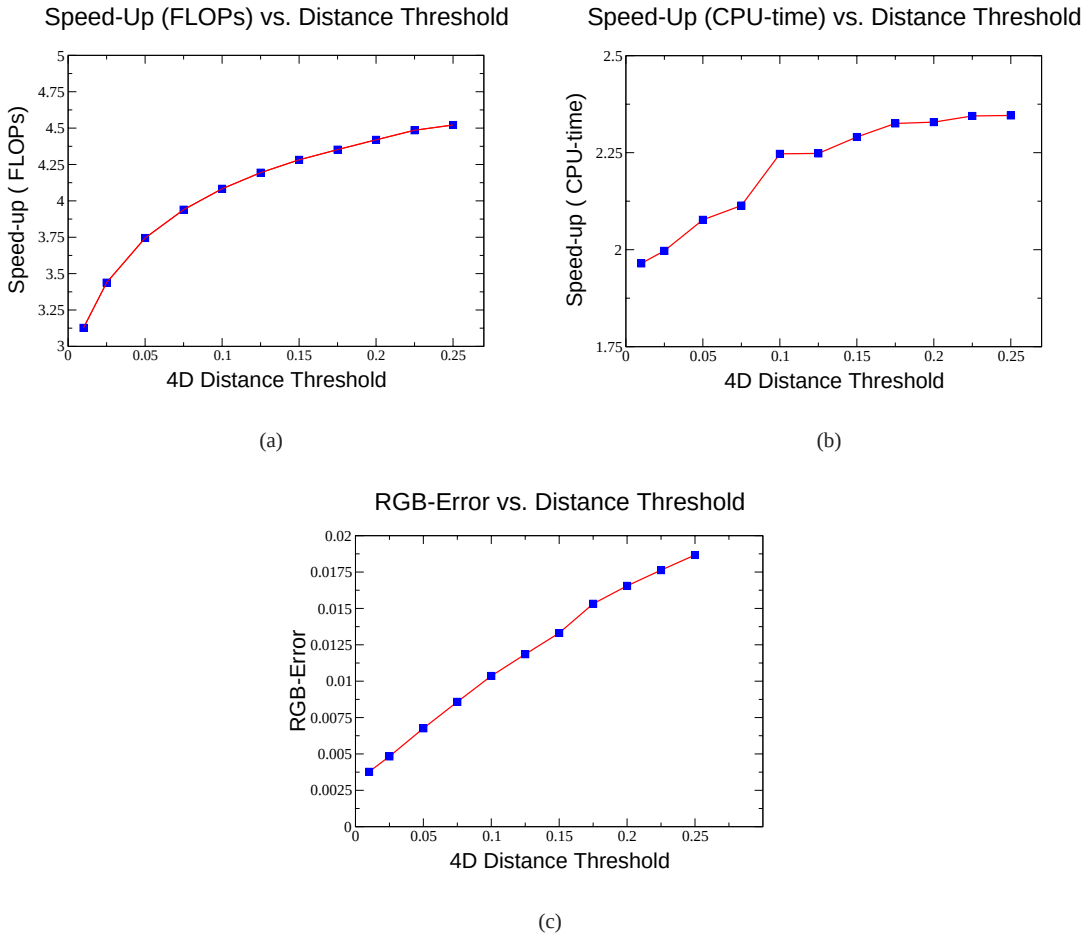

Figure 5: Varying the distance threshold. (angular threshold = $30°$, maximum tree depth = 28, 600×600 image, non-antialiased). Note that the y-axis does not always start at 0.

is greater than 3. These speedups can be quite significant for ray-tracing, where a single frame can take a long time to render.

Fig. 10 (b) and (c) demonstrate how the variation in error reflects the changes in the quality of the rendered image. Notice the blockiness in part (c) when the data structure is not subdivided as densely as in part (b).

3.4 Varying the Angular Threshold The angular threshold, described in Section 2.5, is applied to each query to determine whether the surface curvature variation is too high to apply interpolation. We investigated the speedup and error as a function of the angular threshold over the renderings of three different random volume scenes. The angular threshold is varied from $5°$ to $30°$. The results are shown in Fig. 6.

For lower thresholds, fewer rays could be interpolated due to distant interpolants, and those rays are traced instead. In this case, the actual error committed is smaller but at the expense of lower speedups. However, the speedups are still acceptable even for low thresholds.

3.5 Varying the Maximum Tree Depth Recall that the maximum tree depth, described in Section 2.3, is imposed to avoid excessive tree depth near discontinuity boundaries. We considered maximum depths ranging from 22 to 30. (Because this is a kd-tree in 4-space, four levels of descent are generally required to halve the the diameter of a cell.) The results for the Bezier surface scenes are shown in Fig. 7. The angular threshold is fixed at $30°$, and the distance threshold is fixed at 0.05.

As the tree is allowed to grow up to a higher depth, rays are sampled with increasing density in the regions where the geometric attributes have greater variation, and thus, error committed by the interpolation algorithm decreases with higher depths. The speedup graph shows a more interesting behavior. Up to a certain depth, the speedup increases with depth. This is due to the fact that for low-depth trees, many of the interpolants cannot pass the angular

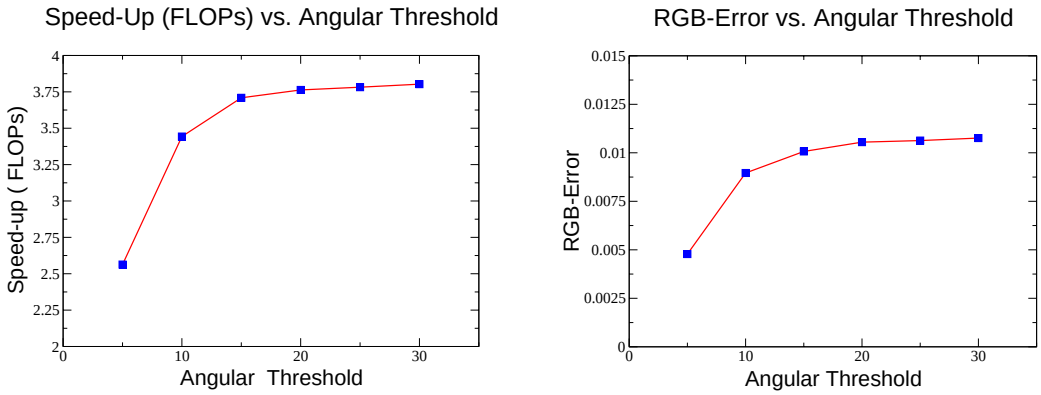

(a) (b)

Figure 6: Varying angular threshold (distance threshold=0.25, maximum depth=28, 300×300, antialiased).

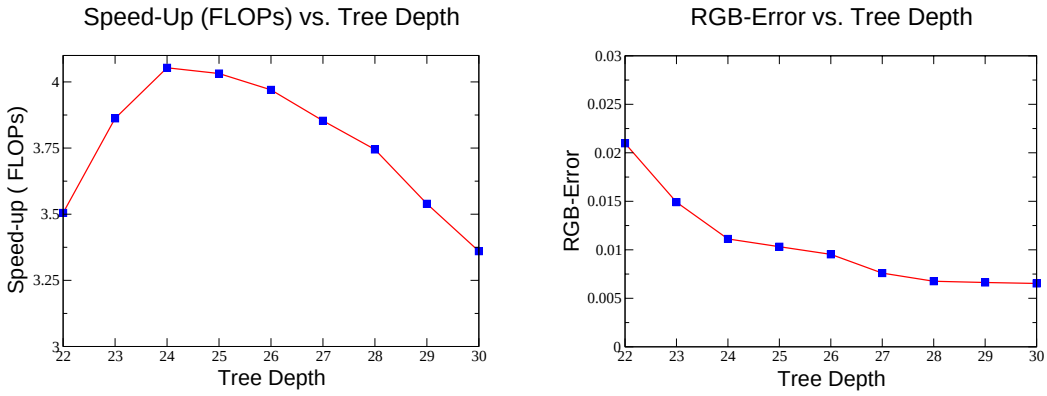

(a) (b)

Figure 7: Varying tree depth (distance threshold=0.05, angular threshold=30, 600×600, non-antialiased).

threshold test, and many rays are being traced rather than interpolated. And so, the speed-ups are low for low-depth trees. Until the peak value of speed-up at some depth value is reached, the performance gain we get from replacing ray-traced pixels by interpolations dominates the overhead of denser sampling. However, with sufficiently large depth values, the speedup decreases as the tree depth becomes higher, since the overhead caused by denser sampling starts dominating.

It seems that a wise choice of depth would be a value that results in both a lower error, and reasonable speedup. For example for the given graph, depth 28 could be a good choice. In addition, Table 2 shows the required memory when depth is varied. When the tree is unnecessarily deep, not only does the speedup decrease, but space requirements increase as well.

3.6 Varying the Cache Size As mentioned earlier, the RI-tree functions as an LRU cache. If an upper limit for the available memory—the cache size—is specified, the least recently used paths are pruned based on time stamps set whenever a path is accessed. Excessively small cache sizes can result in frequent regeneration of the same cells. For the Bezier surface scene, we have varied the cache size from 0.128 to 2.048 megabytes (MB). The resulting speedup graph is shown in Fig. 8.

Notice that we used small cache sizes to demonstrate the sudden increase in speedup as the cache size approaches a reasonable value. Normally, we set the cache size to 100MB which is high enough to handle bigger scenes with many data structures. There are additional parameters involved in garbage collection, such as what percentage of the cache should be pruned. In these experiments, each garbage

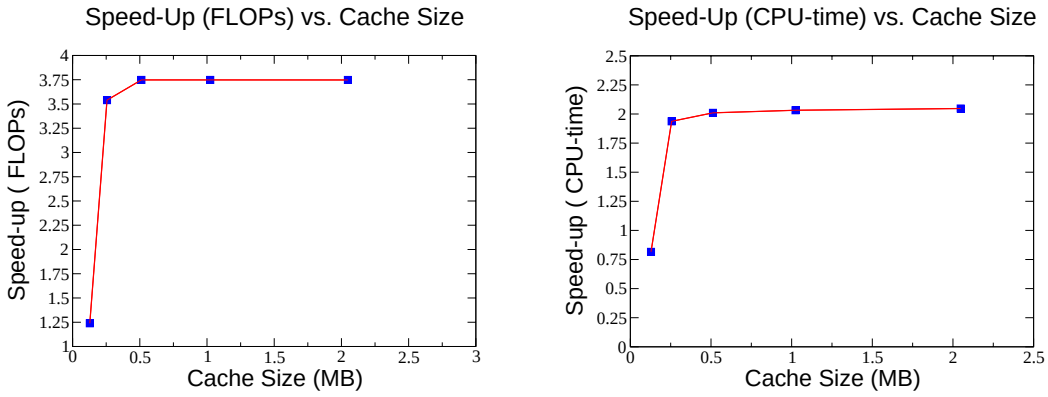

(a) (b)

Figure 8: Varying cache size (distance threshold = 0.05, angular threshold = 30, maximum tree depth = 28, 600×600 image, non-antialiased).

Dist Thresh	Ang Thresh	Tree Depth	Speedup (FLOP)	Speedup(CPU-time)	Error	Memory (MB)
0.25	30	28	2.65	1.89	0.00482	34
0.05	10	28	2.40	1.63	0.00190	47

Table 1: Sample results for tomatoes scene (1200×900 non-antialiased).

collection prunes 70% of the cache.

3.7 Volume Visualization Experiments We have tested the algorithm for the volume visualization application using the same random volumes we have used for refractive objects. Images are 600×600 and not antialiased. Sample run results are shown in Table 2. The FLOP speedup varies from 2.817 to 3.549, and CPU speedup varies from 2.388 to 2.814. For higher resolutions, or anti-aliased images the speedups could be higher. The error could be as low as 0.008 for low distance thresholds, and is still at a reasonable value for higher thresholds. Fig. 12 shows the actual image, and the interpolated image visualizing one of the random volume scenes. All objects have 0.5 opacity, and all have solid gray colors.

3.8 Performance and Error for Tomatoes Scene Finally, we have tested the algorithm on the tomatoes scene generating an image of size 1200×900, non-antialiased. Table 1 shows sample results for the tomato scene and Fig. 9 shows the corresponding images. Fig. 9(a) shows the ray-traced image. Part (b) shows the interpolated image, and a corresponding color-coded image in which the white regions denote the pixels that were traced rather than interpolated. Part (c) shows the interpolated image generated with lower thresholds and the corresponding color-coded image. Notice that the artifacts in part (b) are corrected in part (c).

Note that the closest objects along the eye rays are correctly determined by interpolation, as are the reflection rays from the wrap and the bowl, and the shadows. The sky is reflected on the wrap. As expected, for lower threshold values we can get a very high quality image and still achieve speedups of 2 or higher. If quality is not the main objective, we can get approximate images at higher speedups. The error given is the average RGB-error as explained above.

References

[1] J. Amanatides. Ray tracing with cones. *Computer Graphics (Proc. of SIGGRAPH 84)*, 18(3):129–135, 1984.

[2] J. Arvo and D. Kirk. Fast ray tracing by ray classification. *Computer Graphics (Proc. of SIGGRAPH 87)*, 21(4):196–205, 1987.

[3] F.B. Atalay and D.M. Mount. Ray interpolants for fast ray-tracing reflections and refractions. *Journal of WSCG (Proc. International Conf. in Central Europe on Comp. Graph., Visualization and Comp. Vision)*, 10(3):1–8, 2002.

[4] K. Bala, J. Dorsey, and S. Teller. Radiance interpolants for accelerated bounded-error ray tracing. *ACM Trans. on Graph.*, 18(3), August 1999.

[5] J. L. Bentley. Multidimensional binary search trees used for associative searching. *Commun. of ACM*, 18(9):509–517, 1975.

[6] J. Bloomenthal. *An Introduction to Implicit Surfaces.* Morgan-Kaufmann, San Francisco, 1997.

[7] J. B. Van de Kamer and J. J. W. Lagendijk. Computation of high-resolution SAR distributions in a head due to a radiating dipole antenna representing a hand-held mobile phone. *Physics in Medicine and Biology*, 47:1827–1835, 2002.

[8] D. S. Ebert, F. K. Musgrave, D. Peachey, K. Perlin, and S. Worley. *Texturing and Modelling*. Academic Press Professional, San Diego, 1998.

[9] J. Foley, A. van Dam, S. Feiner, and J. Hughes. *Computer Graphics Principles and Practice*. Addison-Wesley, Reading, Mass., 1990.

[10] A. Gershun. The light field. *Journal of Mathematics and Physics*, XVIII:51–151, 1939. Moscow, 1936, Translated by P. Moon and G. Timoshenko.

[11] A. S. Glassner. Space subdivision for fast ray tracing. *IEEE Comp. Graph. and Appl.*, 4(10):15–22, October 1984.

[12] A. S. Glassner(editor). *An Introduction to Ray Tracing*. Academic Press, San Diego, 1989.

[13] S. J. Gortler, R. Grzeszczuk, R. Szeliski, and M. F. Cohen. The lumigraph. *Computer Graphics (Proc. of SIGGRAPH 96)*, pages 43–54, August 1996.

[14] P. S. Heckbert and P. Hanrahan. Beam tracing polygonal objects. *Computer Graphics (Proc. of SIGGRAPH 84)*, 18(3):119–127, July 1984.

[15] M. R. Kaplan. Space tracing a constant time ray tracer. *State of the Art in Image Synthesis (SIGGRAPH 85 Course Notes)*, 11, July 1985.

[16] M. Levoy and P. Hanrahan. Light field rendering. *Computer Graphics (Proc. of SIGGRAPH 96)*, pages 31–42, August 1996.

[17] P. Moon and D. E. Spencer. *The Photic Field*. MIT Press, Cambridge, 1981.

[18] M. Ohta and M. Maekawa. Ray coherence theorem and constant time ray tracing algorithm. *Computer Graphics 1987 (Proc. of CG International '87)*, pages 303–314, 1987.

[19] S. Rubin and T. Whitted. A three-dimensional representation for fast rendering of complex scenes. *Computer Graphics (Proc. of SIGGRAPH 80)*, 14(3):110–116, July 1980.

[20] H. Samet. *The Design and Analysis of Spatial Data Structures*. Addison-Wesley, 1989.

[21] D. M. Y. Sommerville. *Analytical Geometry in Three Dimensions*. Cambridge University Press, Cambridge, 1934.

[22] D. Zorin, P. Schröder, and W. Sweldens. Interpolating subdivision for meshes with arbitrary topology. *Computer Graphics (Proc. of SIGGRAPH 96)*, pages 189–192, 1996.

Test Input	Dist Thresh	Speedup (FLOP)	Speedup(CPU-time)	Error	Memory (MB)
Bezier Surface	0.010	3.12704	1.96466	0.00377	2.925
	0.025	3.43796	1.99712	0.00483	2.371
	0.050	3.74473	2.07705	0.00676	1.931
	0.075	3.93950	2.11372	0.00858	1.699
	0.100	4.08325	2.24707	0.0103	1. 549
	0.125	4.19358	2.24816	0.01185	1.442
	0.150	4.28194	2.29041	0.01331	1.361
	0.175	4.35214	2.32532	0.01532	1.301
	0.200	4.41940	2.32863	0.01655	1.253
	0.225	4.48503	2.34465	0.01763	1.212
	0.250	4.52146	2.34591	0.01867	1.185
Random Volumes	0.010	3.12173	2.63532	0.00627	19.252
(ray-tracing)	0.025	3.26194	2.64317	0.00645	17.518
	0.050	3.40527	2.71941	0.00679	15.799
	0.075	3.49906	2.76194	0.00722	14.765
	0.100	3.56870	2.79244	0.00780	14.088
	0.125	3.62689	2.84409	0.00853	13.603
	0.150	3.67422	2.88046	0.00890	13.183
	0.175	3.70776	2.89190	0.00945	12.875
	0.200	3.74041	2.92770	0.00989	12.583
	0.225	3.77341	2.94416	0.01048	12.331
	0.250	3.80292	2.91917	0.01076	12.094
Random Volumes	0.050	2.95084	2.42804	0.00850	11.773
(volume	0.150	3.31043	2.67274	0.01179	9.503
visualization)	0.250	3.54958	2.81416	0.01488	8.344
Test Input	Tree Depth	Speedup (FLOP)	Speedup(CPU-time)	Error	Memory (MB)
Bezier Surface	22	3.50486	2.05642	0.02098	0.565
	23	3.86223	2.14654	0.01491	0.706
	24	4.05344	2.21946	0.01112	0.881
	25	4.03178	2.17521	0.01032	1.084
	26	3.97010	2.15906	0.00953	1.318
	27	3.85335	2.05680	0.00760	1.603
	28	3.74473	2.07705	0.00676	1.931
	29	3.53944	2.04811	0.00663	2.265
	30	3.36016	1.97434	0.00653	2.629
Random Volumes	22	3.10450	2.56453	0.01859	3.729
(ray-tracing)	23	3.41967	2.63197	0.01708	4.431
	24	3.70909	2.74675	0.01526	5.441
	25	3.85445	2.90357	0.01449	6.560
	26	3.85108	2.93271	0.01305	7.989
	27	3.84435	2.87188	0.01187	9.660
	28	3.80292	2.91917	0.01076	12.094
	29	3.56893	2.79997	0.01026	14.361
	30	3.34045	2.73197	0.00987	17.413
Input Scene	Ang Thresh	Speedup (FLOP)	Speedup(CPU-time)	Error	
Bezier Surface	5	2.68103	1.68226	0.00424	
	10	3.51840	2.01129	0.00591	
	15	3.68553	2.11734	0.00663	
	20	3.72731	2.12195	0.00673	
	25	3.74471	2.11754	0.00676	
	30	3.74473	2.07705	0.00676	
Random Volumes	5	2.56317	2.15410	0.00478	
(ray-tracing)	10	3.44274	2.67800	0.00896	
	15	3.70928	2.83973	0.01007	
	20	3.76320	2.88208	0.01055	
	25	3.78206	2.89311	0.01063	
	30	3.80292	2.91917	0.01076	
Random Volumes	10	2.81703	2.38833	0.01047	
(volume	15	3.21517	2.62693	0.01340	
visualization)	20	3.40653	2.73348	0.01411	
	30	3.54958	2.81416	0.01488	

Table 2: Speedup and actual error on Bezier Surface and Random Volumes (ray-tracing and volume visualization) for various parameter values.

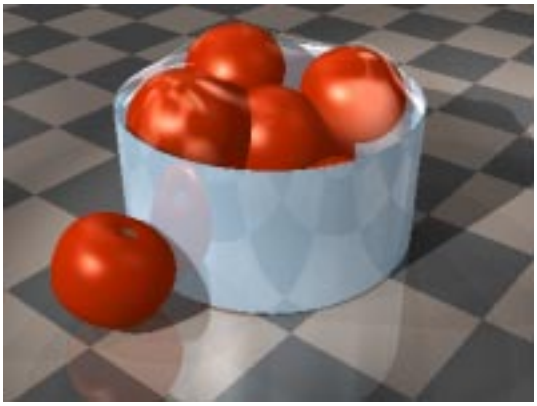

(a)

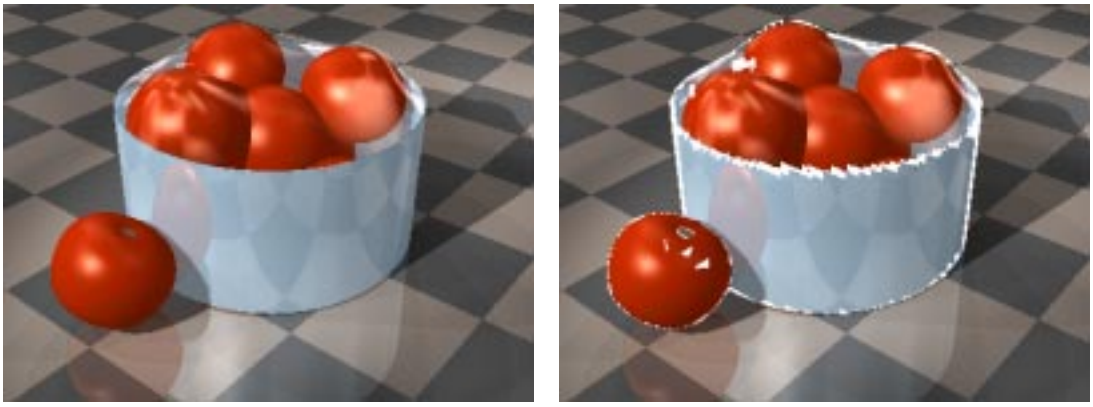

(b)

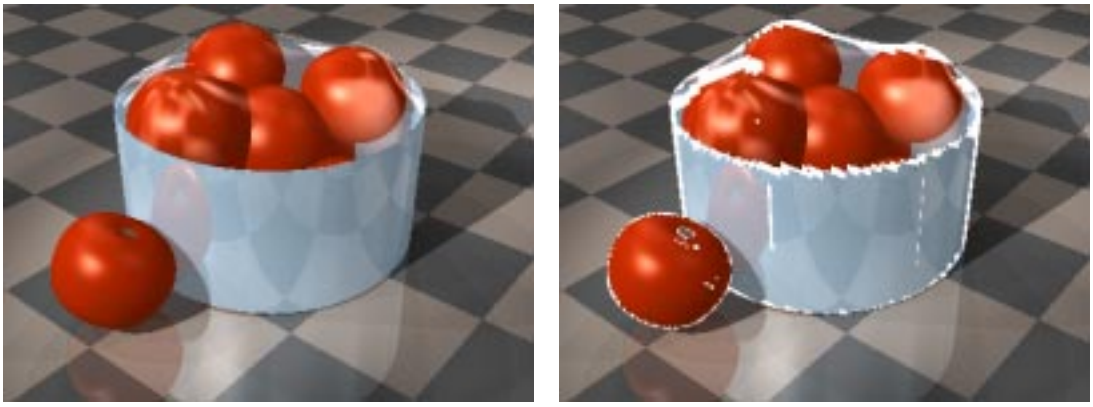

(c)

Figure 9: (a) Ray-traced image, (b) Interpolated image (distance threshold=0.25, angular threshold=30) and corresponding color-coded image, white areas show the ray-traced regions, (c) Interpolated image (distance threshold=0.05, angular threshold=10) and corresponding color-coded image, showing ray-traced pixels.

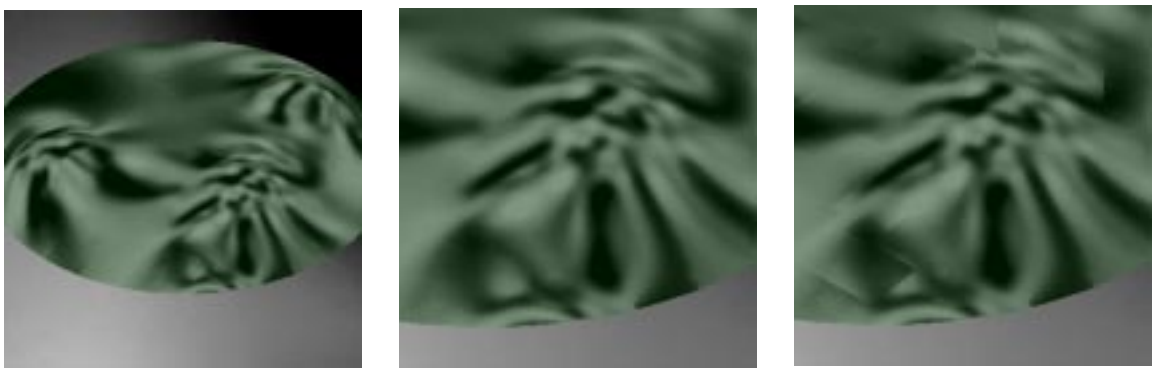

(a) (b) (c)

Figure 10: (a) Ray-traced image, (b) Lower right part of interpolated image (distance threshold=0.01), error = 0.00377, (c) Lower right part of interpolated image (distance threshold=0.15), error = 0.01331.

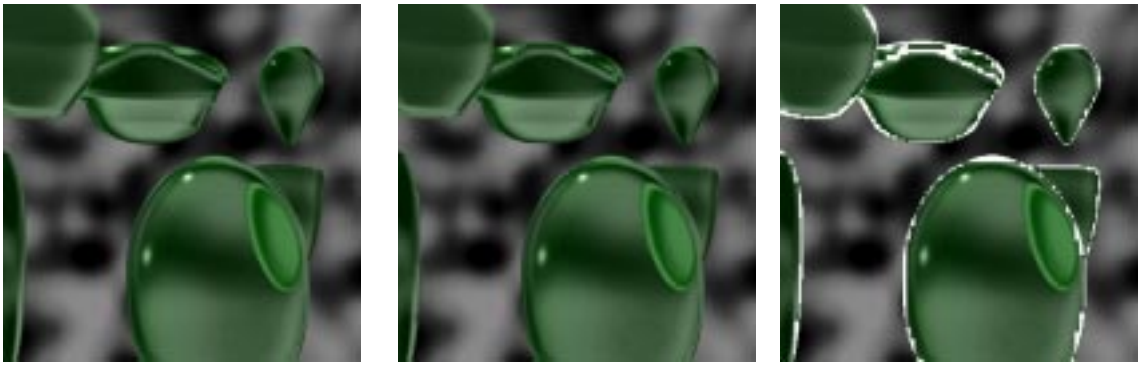

(a) (b)

Figure 11: (a) Ray-traced image, (b) Interpolated image (distance threshold=0.05) and the corresponding color-coded image where white regions indicate pixels that were ray-traced.

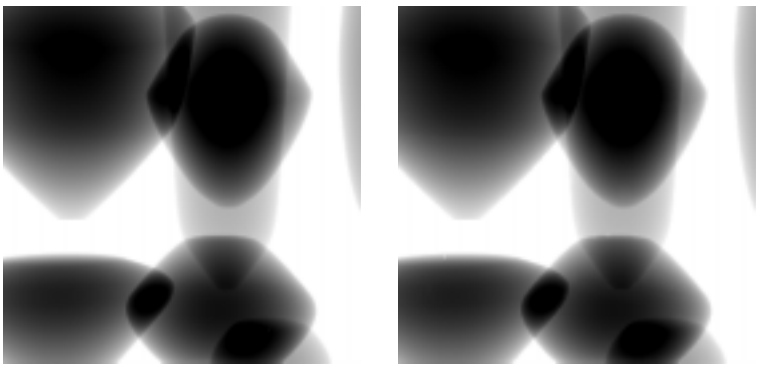

(a) (b)

Figure 12: (a) Ray-traced image, (b) Interpolated image (distance threshold=0.25).